Profiling the Thermoelectric Power of Semiconductor Junctions with Nanometer Resolution

Ho-Ki Lyeo,[1] A. A. Khajetoorians,[1] Li Shi,[2,3]* Kevin P. Pipe,[4] Rajeev J. Ram,[4] Ali Shakouri,[5] C. K. Shih[1,3]*

We have probed the local thermoelectric power of semiconductor nanostructures with the use of ultrahigh-vacuum scanning thermoelectric microscopy. When applied to a *p-n* junction, this method reveals that the thermoelectric power changes its sign abruptly within 2 nanometers across the junction. Because thermoelectric power correlates with electronic structure, we can profile with nanometer spatial resolution the thermoelectric power, band structures, and carrier concentrations of semiconductor junctions that constitute the building blocks of thermoelectric, electronic, and optoelectronic devices.

Thermoelectric coolers and power sources realize energy conversion between heat and electricity without the use of moving mechanical components or hazardous working fluids. Developing new thermoelectric materials with high figures of merit (*ZT*) has been a topic of great interest; a *ZT* larger than 3 will allow thermoelectric coolers to have a coefficient of performance comparable to that of a kitchen refrigerator (*1–3*). Until recently, the *ZT* of the best bulk thermoelectric materials has remained at a value of about 1. The emergence of nanotechnology creates new opportunities to design nanostructured materials for achieving high *ZT* (*4*, *5*). Recent reports of *ZT* improvement to values up to 2.4 with the use of quantum well (*6*) and quantum dot (*7*) superlattices have stimulated much excitement.

ZT is defined as $(S^2\sigma/\kappa)T$, where S is the thermoelectric power or Seebeck coefficient, σ and κ are the electrical and thermal conductivities, respectively, and T is absolute temperature. Understanding the effects of low dimensions and nanoscale structures on S, σ, and κ plays a key role in the rational design of nanostructured thermoelectric materials. The ability to directly measure these thermoelectric properties at the nanoscale should facilitate the development of this field.

We report a direct profiling of S across a semiconductor *p-n* junction with nanometer resolution with the use of scanning thermoelectric microscopy (SThEM). In addition to the divergence and abrupt sign change of S across the electronic junction, we find a direct correlation between the average interdopant spacing and the minimum length scale at which S can be measured in doped semiconductors. Because S is governed by local carrier statistics, SThEM allows us to profile precise electronic junction locations and local carrier concentrations with nanometer resolution, a prominent characterization issue that has challenged the semiconductor industry for many years (*8*).

Our experiment uses an ultrahigh-vacuum (UHV) scanning tunneling microscope (STM) with a base pressure of 5×10^{-11} torr. A heater wire attached to the sample holder is used to raise the sample temperature to 5 to 30 K above room temperature. As the room-temperature tip makes a nanoscale contact with the heated sample, a localized temperature gradient is created in the sample near the contact point (Fig. 1A). This temperature gradient generates a thermoelectric voltage that is directly related to the local S. The setup shares some similarities with the scanning chemical potential microscope (*9*, *10*), but there are two critical differences. First, in our measurement of the thermoelectric voltage, the tip and the sample are in direct nanocontact. We find this to be necessary for obtaining a stable measurement of the thermoelectric voltage on a semiconductor sample (Fig. 1B) (*11*). Second, our measurement is conducted in UHV, avoiding heat conduction through the air gap between the STM tip and the sample. This is crucial for confining the temperature gradient near the tip-sample contact in order to achieve nanometer spatial resolution.

The temperature gradient leads to a thermoelectric voltage,

$$V(x, y) = S(x, y)(T_c - T_1) \qquad (1)$$

where T_c and T_1 are the temperatures of the contact and the back side of the sample, respectively, and $S(x, y)$ is the spatial average within the nonuniform temperature zone localized in the semiconductor sample. The S of the metal tip and the lead wires is ignored because it is much smaller than that of the semiconductor sample.

An STM image is shown across an atomically flat GaAs *p-n* junction in Fig. 2 (inset). The height contrast in the STM image is reversed as the polarity of the STM bias is reversed. Whereas the boundary between the dark and bright regions roughly corresponds to the junction location, the apparent junction location in the STM images can shift as much as 20 nm, depending on the bias condition. As discussed extensively in previous work (*12–14*), this is due to a tip voltage–induced band-bending effect and is responsible for the uncertainty in locating the precise *p-n* junction location by means of STM.

[1]Department of Physics, [2]Department of Mechanical Engineering, [3]Center for Nano and Molecular Science and Technology, University of Texas, Austin, TX 78712, USA. [4]Research Laboratory of Electronics, Massachusetts Institute of Technology, Cambridge, MA 02139, USA. [5]Department of Electrical Engineering, University of California, Santa Cruz, CA 95064, USA.

*To whom correspondence should be addressed. E-mail: lishi@mail.utexas.edu, shih@physics.utexas.edu

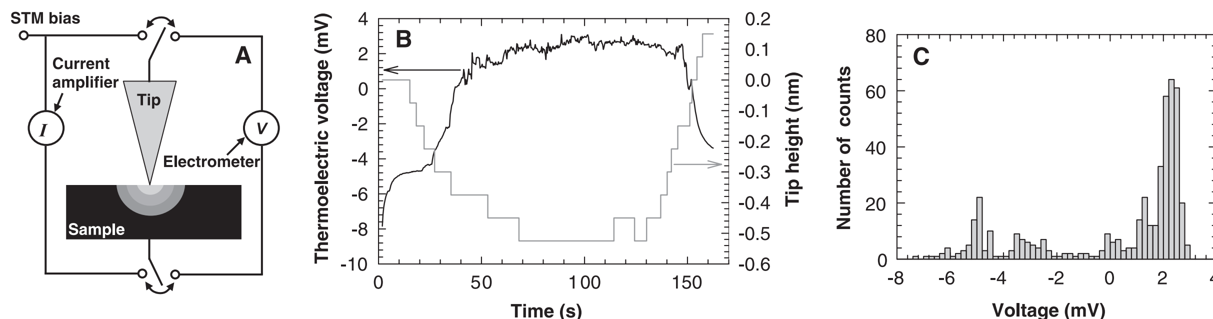

Fig. 1. (**A**) Schematic of the SThEM setup showing a nonuniform temperature zone in the sample. (**B**) Time profiles of the measured voltage and the tip height as the tip approaches the sample, then retracts. (**C**) Histogram of the measured voltage.

The S profile across the junction (Fig. 2) calculated from the band structure was obtained using the depletion approximation based on the dopant profile measured by secondary ion mass spectroscopy (SIMS) (*11*, *15*). The calculated S profile exhibits an abrupt polarity inversion near the junction: The separation between the positive peak value and the negative one is only 1.2 nm. The reason for this sudden sign inversion is that, under the assumption of a continuous distribution of dopant atoms, the majority carrier type changes abruptly near the junction because a band bending of a few $k_B T$ (where k_B is the Boltzmann constant) occurs within 1 nm of the junction.

The SThEM measurement result is also plotted in Fig. 2. On either side of the junction, the magnitude of the measured thermoelectric voltage increases toward the junction, continuing until about 4 nm from the junction, where the magnitude decreases because the contribution of the minority carriers cancels that of the majority ones. Furthermore, the voltage changes its sign across the junction as a result of the inversion of the majority carrier type. The sign reversal occurs within 2 nm, whereas the distance between the positive and negative peaks is about 8 nm. The measured thermoelectric voltage profile—in particular, the divergence near the junction and the abrupt sign change across the junction—agrees qualitatively with the calculated S profile. However, the calculated profile shows much sharper transition at the junction.

The discrepancy can be attributed to the breakdown of the continuum assumption for the calculation of S at a length scale comparable to the average interdopant spacing (i.e., 4.6 nm), corresponding to a dopant concentration of about 10^{19} cm^{-3}. Further, it also reveals the spatial resolution of the measurement, which is limited not only by the contact size (1 nm or less) but also by the size of the nonuniform temperature zone.

We note that the peak-to-peak distance of the measured thermoelectric profile is about twice the average interdopant spacing. To further examine this correlation, we performed experiments on p-n junctions with different doping levels. The thermoelectric voltage profile was measured on another GaAs sample consisting of a p layer sandwiched between two n layers (Fig. 3). Compared to the calculated S profile, the measured profile shows a broadening effect with a distance of ~20 nm between the positive peak and the negative one. This distance is again roughly twice the 10-nm interdopant spacing in the p layer.

This observation suggests that the size of the nonuniform temperature zone is defined by impurity scattering to be about twice the interdopant spacing in the highly doped semiconductor. This idea is supported by an experiment showing that the phonon mean free path (λ_{ph}) in a doped GaAs sample scales with the average interdopant spacing, measuring 13.3, 6.2, and 2.88 nm for a dopant concentration of 10^{17}, 10^{18}, and 10^{19} cm^{-3}, respectively (*16*). Because phonons are the dominant heat carriers in the semiconductor sample, one thus expects that in spherical geometry the temperature rise decays as $\Delta T \sim \lambda_{ph}/r$ for $r > \lambda_{ph}$, where r is the distance from the contact. Hence, the size of the nonuniform temperature zone should be about a factor of 2 to 3 greater than λ_{ph}, or about two to three times the interdopant spacing if the values in (*16*) are used. Still, the nonuniform temperature zone needs to be larger than the electron-phonon scattering mean free path for electrons and phonons to establish local thermal equilibrium in this zone. In a highly doped semiconductor, one expects that the electron mean free path is comparable to the average interdopant spacing because of scattering with ionized impurities. Although impurity scattering is an elastic process and has no direct impact on the electron-phonon scattering mean free time, it alters the electron trajectory and reduces the effective electron-phonon scattering mean free path to be comparable to the interdopant spacing. Hence, electrons and phonons also establish local thermal equilibrium at the length scale of the interdopant spacing, allowing us to profile local S at a length scale of about two to three times the interdopant spacing. Moreover, this method can potentially be applied to directly probe the local S of individual quantum wells and wires, where the nonuniform temperature zone can be further confined within the nanostructures by interfaces.

Inside the nonuniform temperature zone, the S can be nonuniform because of the presence of a depletion zone from the formation of a tip-sample Schottky junction. However, the depletion width of the nanoscale Schottky junction is much smaller than that of a planar one, and this width is comparable to the interdopant spacing (*17*, *18*). Because λ_{ph} is also comparable to the interdopant spacing, the temperature rise within much of the depletion zone should be only a small fraction of the total value. Experimentally, neglecting the temperature rise in the tip because of its high thermal conductivity, we find the measurement results to be about 80% of the bulk values. Considering a small temperature rise in the tip, one can expect that the measurement results are rather close to the bulk property. Although our observation suggests that the depletion zone and other effects, such as the suppression of the phonon-drag thermoelectric power at a nanocontact (*19*–*21*), do not cause large measurement errors, this method allows further investigation of these intriguing nanoscale effects.

In Fig. 4, we directly convert the measured S profile to the band structure and carrier profile (*11*). The band structure calculated from the SIMS dopant profile and the carrier profile calculated from the band structure by Fermi-Dirac statistics are also shown for comparison. The results from SIMS and SThEM exhibit good

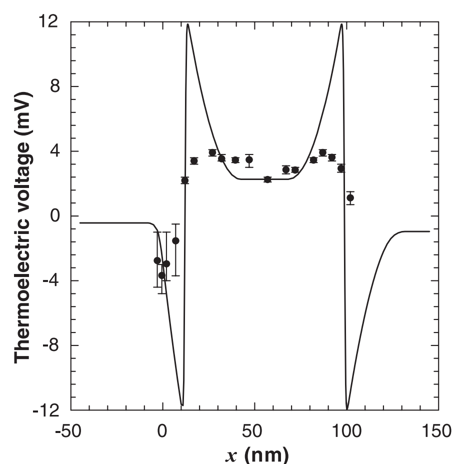

Fig. 3. Measured thermoelectric voltage (circles) and calculated S multiplied by 5 K (line) of a GaAs sample consisting of a p-type layer, 100 nm thick, sandwiched between two n-type layers. The p-type layer is doped with Be at 1×10^{18} cm^{-3}; the n-type layers to the left and right are doped with Si at 5×10^{18} cm^{-3} and 1×10^{18} cm^{-3}, respectively. x is measured from the left p-n junction.

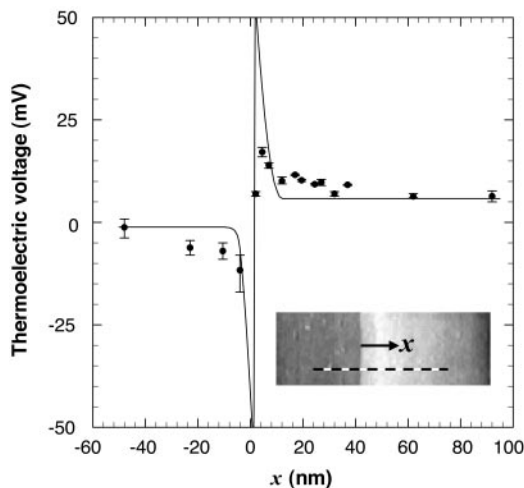

Fig. 2. Measured thermoelectric voltage (circles) and calculated S multiplied by 22 K (line) across a GaAs p-n junction as a function of distance (x). The sample was heated 30 K above the tip (room) temperature. Because of the temperature rise in the tip and in a depletion zone within the nonuniform temperature zone, the value of 22 K yields a better agreement than 30 K between the measurement and the calculation. Inset: STM image of the junction (filled state with a sample bias of –2 V). The bright strip is p-doped with Be at 9×10^{18} cm^{-3}, and the dark strip is n-doped with Si at 1.1×10^{19} cm^{-3}. The dashed line is 150 nm, corresponding to the line where voltage profile is measured.

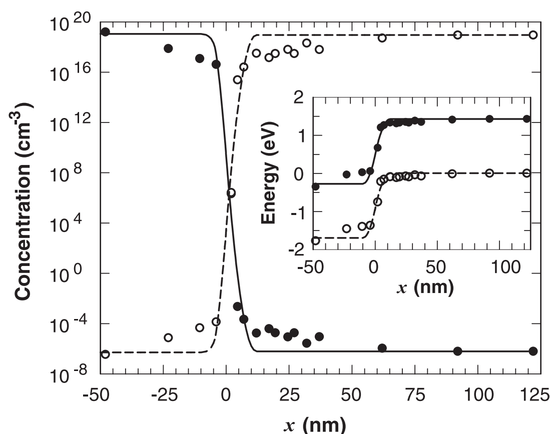

Fig. 4. Carrier profile across the *p-n* junction shown in Fig. 2. Solid and dashed lines are electron and hole concentrations, respectively, calculated from the SIMS dopant profile. Solid and open circles are electron and hole concentrations, respectively, calculated from the SThEM results. Inset: Energy diagram of the *p-n* junction. Solid and open circles are the conduction and valence band edge, respectively, calculated from the SThEM results. Solid and dashed lines are calculated from the SIMS dopant profile.

agreement, although the match is poor at the edges of the depletion region (likely as a result of the continuum assumption and the depletion approximation invoked for the calculation based on SIMS). An important feature is the ability of SThEM to resolve the location of the electronic junction to within 2 nm. This position corresponds to the location where the majority carrier type changes, resulting in the abrupt sign change of the thermoelectric voltage. Because there is no external electrical bias across the tip-sample junction, the SThEM measurement does not suffer the severe tip voltage–induced band-bending effect that exists in STM or scanning capacitance microscopy, where a very large external electric field ($\sim 10^9$ V/m) exists at the tip-sample gap and shifts the junction location. The resolution shown here for junction delineation shows a significant improvement over most of the characterization techniques available today.

References and Notes

1. G. Mahan, B. Sales, J. Sharp, *Phys. Today* **50**, 42 (1997).
2. F. J. DiSalvo, *Science* **285**, 703 (1999).
3. H. Edwards, Q. Niu, A. de Lozanne, in *Wiley Encyclopedia of Electrical and Electronics Engineering*, J. G. Webster, Ed. (Wiley, New York, 1999), vol. 22, pp. 80–90.
4. L. D. Hicks, M. S. Dresselhaus, *Phys. Rev. B* **47**, 12727 (1993).
5. L. D. Hicks, M. S. Dresselhaus, *Phys. Rev. B* **47**, 16631 (1993).
6. R. Venhatasubramanian, E. Siivola, T. Colpitts, B. O'Quinn, *Nature* **413**, 597 (2001).
7. T. C. Harman, P. J. Taylor, M. P. Walsh, B. E. LaForge, *Science* **297**, 2229 (2002).
8. P. de Wolf, R. Stephenson, T. Trenkler, T. Hantschel, W. Vandervorst, *J. Vac. Sci. Technol. B* **18**, 361 (2000).
9. C. C. Williams, H. K. Wickramasinghe, *Nature* **344**, 317 (1990).
10. J. C. Poler, R. M. Zimmermann, E. C. Cox, *Langmuir* **11**, 2689 (1995).
11. See supporting data on *Science* Online.
12. A. Vaterlaus, R. M. Feenstra, P. D. Kirchner, J. M. Woodall, G. D. Pettit, *J. Vac. Sci. Technol. B* **11**, 1502 (1993).
13. A. R. Smith *et al.*, *J. Vac. Sci. Technol. B* **12**, 2610 (1994).
14. N. D. Jäger *et al.*, *Phys. Rev. B* **67**, 165307 (2003).
15. K. P. Pipe, R. J. Ram, A. Shakouri, *Phys. Rev. B* **66**, 125316 (2002).
16. J. F. Bresse, A. C. Papadopoulo, *J. Appl. Phys.* **64**, 98 (1988).
17. G. D. J. Smit, S. Rogge, T. M. Klapwilk, *Appl. Phys. Lett.* **81**, 3852 (2002).
18. For a planar junction, the depletion width (W) is related to the barrier height (φ) as $W = (2\varphi\varepsilon_s/e^2N)^{1/2}$, where ε_s is the dielectric constant and N is the doping density. For a point contact of a hemispherical contact area with a radius of a_o, we obtain the radius of hemispherical depletion zone as $r_o \approx (3a_o\varepsilon_s\varphi/e^2N)^{1/3}$, provided that $a_o \ll r_o$. Using $a_o = 1$ nm, $\varphi = 0.5$ eV, and $N = 10^{19}$/cm^3, we find that $r_o \sim 5$ nm. Note that in the derivation we assume a uniform and continuous charge distribution. However, r_o is now very close to the average interdopant spacing, and one expects that this assumption breaks down. Nonetheless, on the basis of the qualitative scaling behavior, one can still conclude that $r_o < W$.
19. R. Trzcinski, E. Gmelin, H. J. Queisser, *Phys. Rev. Lett.* **56**, 1086 (1986).
20. O. I. Shklyareskii, A. G. M. Jansen, J. G. H. Hermsen, P. Wyder, *Phys. Rev. Lett.* **57**, 1374 (1986).
21. L. Weber, M. Lehr, E. Gmelin, *Phys. Rev. B* **46**, 9511 (1992).
22. Supported by NSF grants DMR-0210383, DMR-0306239, and CTS-0239179 and by the Texas Advanced Technology Program. L.S. thanks U. Ghoshal for helpful discussions on SThEM.

Supporting Online Material
www.sciencemag.org/cgi/content/full/303/5659/816/DC1
Materials and Methods
References

17 September 2003; accepted 11 December 2003

Cubic $AgPb_mSbTe_{2+m}$: Bulk Thermoelectric Materials with High Figure of Merit

Kuei Fang Hsu,[1] Sim Loo,[2] Fu Guo,[2] Wei Chen,[3] Jeffrey S. Dyck,[3] Ctirad Uher,[3] Tim Hogan,[2] E. K. Polychroniadis,[4] Mercouri G. Kanatzidis[1]*

The conversion of heat to electricity by thermoelectric devices may play a key role in the future for energy production and utilization. However, in order to meet that role, more efficient thermoelectric materials are needed that are suitable for high-temperature applications. We show that the material system $AgPb_mSbTe_{2+m}$ may be suitable for this purpose. With $m = 10$ and 18 and doped appropriately, *n*-type semiconductors can be produced that exhibit a high thermoelectric figure of merit material ZT_{max} of ~2.2 at 800 kelvin. In the temperature range 600 to 900 kelvin, the $AgPb_mSbTe_{2+m}$ material is expected to outperform all reported bulk thermoelectrics, thereby earmarking it as a material system for potential use in efficient thermoelectric power generation from heat sources.

Thermoelectric devices are generally based on heavily doped semiconductors and can be used for cooling applications or for electricity generation directly from a heat source. When supplied by a temperature differential, thermoelectric semiconductors respond by virtue of the Seebeck effect to produce a voltage that could be used to drive an external load. A broad search has been under way to identify new materials with enhanced thermoelectric properties. Although the emphasis has been on finding materials that are superior to the well-known $Bi_{2-x}Sb_xTe_{3-y}Se_y$ alloys used in cooling, interest in developing materials with high ZT values (*1*) at high temperatures for direct energy conversion has been increasing. Several classes of materials are currently under investigation, including complex chalcogenides (*2*), skutterudites (*3*, *4*), half-Heusler alloys (*5*), metal oxides (*6*), intermetallic clathrates (*7*–*9*), and pentatellurides (*10*). In addition, artificial superlattice thin-film structures grown from chemical vapor deposition, such as Bi_2Te_3/Sb_2Te_3 (*11*), and by molecular beam epitaxy (MBE), such as $PbSe_{0.98}Te_{0.02}$/PbTe (*12*, *13*), have been introduced with substantially enhanced ZT values relative to those of their bulk counterparts. Marking an important development in this area, specially constructed Bi_2Te_3/Sb_2Te_3 superlattices were reported to exhibit a very high ZT of ~2.4 at room temperature (*14*). The MBE-grown thin-film $PbSe_{0.98}Te_{0.02}$/PbTe systems (*11*, *12*) feature peculiar pyramidal-shaped "nanodots" of PbSe that form spon-